The Astrophysical Journal, 614:1054–1062, 2004 October 20

ON THE RELATION BETWEEN FILAMENT ERUPTIONS, FLARES, AND CORONAL MASS EJECTIONS

Ju Jing, Vasyl B. Yurchyshyn, Guo Yang, Yan Xu, and Haimin Wang
New Jersey Institute of Technology, Center for Solar-Terrestrial Research, 323 Martin Luther King Boulevard, Newark, NJ 07102; jj4@njit.edu
Received 2004 March 24; accepted 2004 June 23

ABSTRACT

We present a statistical study of 106 filament eruptions, which were automatically detected by a pattern recognition program implemented at Big Bear Solar Observatory using Hα full-disk data from 1999 to 2003. We compare these events with *Geostationary Operational Environmental Satellite* soft X-ray time profiles, solar-geophysical data (SGD) solar event reports, Michelson Doppler Imager magnetograms, and Large Angle and Spectrometric Coronagraph (LASCO) data to determine the relationship between filament eruptions and other phenomena of solar activity. (1) Excluding eight events with no corresponding LASCO data, 55% or 56% of 98 events were associated with coronal mass ejections (CMEs). (2) Active region filament eruptions have a considerably higher flare association rate of 95% compared to quiescent filament eruptions with 27%, but a comparable CME association rate, namely, 43% for active region filament eruptions and 54% for quiescent filament eruptions. (3) 54% or 68% of 80 disk events were associated with new flux emergence. In addition, we derived the sign of magnetic helicity and the orientation of the magnetic field associated with seven halo CMEs and demonstrated that the geoeffectiveness of a halo CME can be predicted by these two parameters.

Subject headings: Sun: corona — Sun: coronal mass ejections (CMEs) — Sun: filaments — Sun: prominences

Online material: machine-readable table

1. INTRODUCTION

Filament eruptions, flares, and coronal mass ejections (CMEs) are the most important solar events as far as space weather effects are concerned, linking solar eruptions, major interplanetary disturbances, and geomagnetic storms (Gosling et al. 1991). A halo CME, which is usually associated with activity near the solar disk center, has great influence on space weather because an Earthward halo CME is indicative of coronal mass and magnetic fields moving out toward the Earth and is therefore likely to cause geoeffective disturbances (Cane et al. 2000; Webb et al. 2000). The sign of magnetic helicity in active regions can be used to predict the orientation of the magnetic field associated with a CME and furthermore the probability of a geomagnetic storm (Yurchyshyn et al. 2001).

In order to gain a better understanding of CMEs and to improve the reliability of geomagnetic storm predictions and warnings, it is essential to observe early manifestations of CMEs in the solar atmosphere. Thus, our goal is to find possible relationships between solar surface phenomena such as filament eruptions and flares, the CMEs' occurrence, and the properties of the associated magnetic field. Once a relationship is found, it can serve as an indicator for the occurrence of geomagnetic storms.

Filaments and prominences refer to the same physical structures on the Sun, either projected onto the disk or extending above the limb. The majority of previous statistical studies regarding the connection between filament (or prominence) eruptions and CMEs have focused on prominences because they could easily be detected, observed, and measured against the dark sky background. Moreover, CMEs, associated with the prominences, are not difficult to detect. Many prominence classifications have been proposed in the past. For example, Gilbert et al. (2000) developed definitions of active prominences (APs) and eruptive prominences (EPs) and studied the relationship between APs, EPs, and CMEs for 54 events. They found that 94% of the EPs had an associated CME compared to only 46% for APs. Gopalswamy et al. (2003) defined a prominence as a radial or a transverse event. Authors showed that the radial events have a strong correlation to the CMEs: 83% of the radial events were associated with CMEs compared to 24% for transverse events. However, Yang & Wang (2002) showed that the connection between filament disappearances observed in Hα spectral line and CMEs is weak, ranging from 10% to 30%.

Filament disappearance does not always imply filament eruptions. Depending on their physical nature, disappearing filaments can reappear. Two processes have been proposed by Mouradian et al. (1995): dynamic sudden disappearance (DSD) and thermal disappearance (THD). DSD is due to restructuring of the magnetic field, and it ultimately leads to the disappearance of the filament through an eruption process, whereas THD is due to heating of the plasma in the filament, which will reappear once it cools down. Since THD is not related to magnetic field reorganization, we excluded it from this study.

We define a "filament eruption" as a solar activity event with significant upward motion and with at least 50% of the material vanishing during the course of a day. In this sense, filament eruptions and the aforementioned DSDs, EPs, and radial events are really all the same manifestations but with slightly different definitions. We should also note that our study includes both filament eruptions observed close to the solar limb with a normalized distance from the solar disk center larger than 0.6 $R_{\odot}$ and Earth-directed filament eruptions observed on the disk. Since we have eliminated the THD events from our study, terms "disappearance" and "eruption" are used synonymously throughout the rest of the paper. Two Big Bear Solar Observatory (BBSO) Hα full-disk images, about 24 hr apart, allow us to identify filament disappearance on the disk. Then we use high-cadence data of Hα and the Extra-Ultraviolet Imaging Telescope (EIT) on board the *Solar and Heliospheric Observatory* (*SOHO*) to confirm these events are indeed erupting, even though their signatures in EIT images are more difficult to identify. A filament is considered to be erupting if it displays ascending motion, in contrast to filaments that fade away as a whole, while their general shape remains the same. The latter type of disappearing filaments has been discarded from our study. Usually, ascending motion of filaments is determined by the line-of-sight velocity derived from Doppler measurements. Unfortunately, we do not have such data. The evolution of the geometrical shape of the filament, for example, whether it shows a loop-like eruption, provides us the clue to determine whether it is actually erupting.

In this paper we present a comprehensive 5 yr study of filament eruptions from 1999 January 1 to 2003 December 31. The study includes both close-to-limb events ($R > 0.6\ R_\odot$) and Earth-directed disk events. We present a statistical study on the relationship between filament eruptions, flares, and CMEs. The data sets are described in § 2, the methods are outlined in § 3, the statistical results are listed in § 4, and finally, the observational results are discussed and summarized in §§ 5 and 6.

2. DATA SETS

We used BBSO Hα full-disk images as the primary data set to detect the filament eruptions. During the last few years, BBSO has developed a new generation of well-calibrated, photometric Hα full-disk observations (Denker et al. 1999; Steinegger et al. 2000), which include limb-darkening correction to enhance features on the disk as well as above the limb. The Hα full-disk data were acquired with a large-format, 2k $\times$ 2k pixels, 14 bit Apogee KX4 CCD camera. The time cadence is one image frame per minute during the entire observing day, and the image scale is approximately 1$''$ pixel^{-1}.

In addition to the Hα observations, Michelson Doppler Imager (MDI) magnetograms (Scherrer et al. 1995), EIT images (Delaboudinière et al. 1995), Large Angle and Spectrometric Coronagraph (LASCO) C2 coronagraphs (Brueckner et al. 1995), *Geostationary Operational Environmental Satellite* (*GOES*) soft X-ray light curves, and solar-geophysical data (SGD) solar event reports were examined to identify the related phenomena of solar activity such as new flux emergence, flares, and CMEs.

3. METHODS

Unlike in some previous studies, which used CMEs as the starting point and traced them back to their origin on the solar surface (Webb & Hundhausen 1987; Webb et al. 2000), we started by identifying a filament disappearance, eliminating those events that are not indeed erupting, and then evaluated *GOES* soft X-ray light curves, SGD solar event reports, MDI magnetograms, and LASCO data to establish a relationship between the filament eruption and other phenomena of solar activity.

3.1. *Data Selection*

A total of 3620 filament disappearance events were detected by an automatic detection program from 1999 January 1 to 2003 December 31, which uses IDL code in a Linux system and generates a "filament disappearance report" every day (Gao et al. 2002). The program selects one Hα snapshot each day and compares it with another image from the previous day in order to detect disappearing filaments. To simplify the data selection, we first selected 243 filament disappearances, with a surface area of at least 2000 arcsec^2. In order to be included in our study list, observations, with the cadence of 1 image frame per minute, have to be available during the entire progress of the filament disappearance. In case there was a data gap in the BBSO Hα full-disk image sequence, we resorted to Hα full-disk images obtained at the Kanzelhöhe Solar Observatory (KSO) in Austria and EIT images that have a relatively lower temporal cadence, 12 minutes. During this process of selection, we were able to exclude some misidentifications made by the program, events that had not been satisfactorily observed, as well as some filament disappearances that could not unambiguously be classified as filament eruptions. Since active region filaments appear to be thinner in depth and width than quiescent filaments, 22 small events ($<$2000 arcsec^2), most of them in active regions, were included in our study as supplementary to filament eruptions in active regions. The final sample of filament eruptions included in this study was 106, 43 of them with complete Hα coverage, while the rest of the events were observed from the beginning to the end in EIT images.

3.2. *Event Classification*

Flares.—Flares (optical and X-ray flares) were identified first as sudden brightenings in Hα (flare ribbons) or EIT (flare loops) observations. In other words, flare association is determined directly from the observation. Then we examined *GOES* soft X-ray flux profiles and SGD solar event reports, within a time period of 1 hr around the observed onset time of flares, for X-ray class, onset time, and location.

New flux emergence.—We determined new flux emergences from a time sequences of MDI magnetograms with a 790$''\times$ 590$''$ field of view (FOV) obtained at least 12 hr prior to the eruption. The FOV was centered on the eruptive filament to locate the magnetic field in the "vicinity of the filament" (see Feynman & Martin 1995 for the definition of the "vicinity of the filament").

CMEs.—We used LASCO C2 coronagraph images and the CME catalog[1] (Gopalswamy et al. 2003) to determine whether there was a CME associated with the filament eruption. We require that the latitude of the CME be within $\pm 30^\circ$ of the latitude of the eruptive filament and that the CME appear in LASCO C2 coronagraph images within 2 hr after the eruption of the filament. We chose this particular time delay because it takes approximately 2 hr for a CME traveling at a relatively low plane-of-sky speed of 200 km s^{-1} to cover a distance of 2 $R_\odot$, i.e., to reach the LASCO C2 FOV. Taking into account the projection effect and the acceleration time of a CME, this 2 hr time window seemed reasonable. For events that originate near disk center and are likely to result in halo or partial halo CMEs, the above requirements have to be relaxed.

4. RESULTS OF FILAMENT ERUPTION ASSOCIATIONS

Table 1 presents a list of 106 filament eruptions and summarizes their relation to emerging flux regions (EFRs), flares, and CMEs. Columns (1) and (2) contain the date and time of the filament eruptions. Subsequent columns provide observed properties of the filament eruptions (position, size, chirality) and relate them to occurrences of EFRs, flares, and CMEs. In the following enumeration, we explain some of the terms used in Table 1.

[1] See http://cdaw.gsfc.nasa.gov.

TABLE 1
PROPERTIES OF FILAMENTS ERUPTIONS AND THEIR ASSOCIATED SOLAR ACTIVITY

	FILAMENTS						FLARES			CMES		
DATE (1)	Eruption Time (UT) (2)	Position (3)	Size (arcsec^2) (4)	Type (5)	Chirality (6)	EFR[a] (7)	Class (8)	Time[b] (UT) (9)	Location (10)	Time[c] (UT) (11)	Central P.A.[d] (deg) (12)	AW[e] (deg) (13)
1999 Jan 17...............	17:32–20:21	N38E16	2612	AR8440	. . .	No data	C2.5	18:29	N18E19	. . .	. . .	. . .
1999 Mar 10	02:00–03:00	S40W16	12080	QS	Dextral	Yes	. . .	. . .	. . .	03:26	176	76
1999 Mar 20	21:12–23:24	N23W07	4260	QS	. . .	No	. . .	. . .	. . .	. . .	. . .	. . .
1999 Mar 23	03:00–06:00	S17E11	1984	QS	Sinistral	Yes	. . .	. . .	. . .	04:54	152	48
1999 Mar 23	03:00–06:00	S36E24	1180	QS	Sinistral	No	. . .	. . .	. . .	04:54	152	48
1999 Apr 18..............	07:13–07:48	N39E07	3768	QS	Dextral	Yes	B3.8	08:40	. . .	08:30	59	>112
1999 May 22.............	06:12–11:12	S12E11	3708	QS	Sinistral	Yes	. . .	. . .	. . .	. . .	. . .	. . .
1999 Jun 8	10:02–11:48	S35E21	2088	QS	Sinistral	Yes	. . .	. . .	. . .	. . .	. . .	. . .
1999 Jun 24	12:48–13:36	N39W08	2808	AR8595	Dextral	Yes	C4.1	12:04	N29W13	13:31	Partial halo	. . .
1999 Jul 1	02:24–04:00	S31W18	2404	QS	Sinistral	Yes	C5.4	01:41	S15W16	. . .	. . .	. . .
1999 Aug 20.............	13:13–16:36	N59W74	6888	QS	. . .	Limb[f]	. . .	. . .	. . .	18:06	346	88
1999 Sep 9................	18:45–21:36	N34W41	6800	QS	Dextral	Yes	. . .	. . .	. . .	19:52	304	73
1999 Sep 12..............	00:24–01:25	S16W52	4176	QS	Sinistral	Limb	. . .	. . .	. . .	00:54	271	121
1999 Sep 16..............	15:48–16:36	N49W44	13744	QS	Dextral	Limb	. . .	. . .	. . .	16:54	Partial halo 6	147
1999 Sep 20..............	04:00–05:00	S21E01	5672	QS	Sinistral	No	C2.8	05:46	. . .	06:06	Very faint halo	360
1999 Oct 13	08:12–09:36	N49E12	12992	QS	Dextral	No	Optical	. . .	. . .	09:50	4	109
1999 Oct 25	13:36–14:12	S36W19	4368	QS	Sinistral	No	C1.2	14:40	. . .	14:26	Partial halo 186	146
1999 Nov 9...............	14:35–15:31	N49E21	3280	QS	Dextral	Yes	. . .	. . .	. . .	No data	. . .	. . .
1999 Nov 26.............	17:08–19:13	S46W04	3596	QS	Sinistral	Yes	C2.3	17:40	S11W08	17:30	Partial halo 228	145
1999 Dec 28	22:00–23:48	S04E17	2368	QS	Sinistral	Yes	. . .	. . .	. . .	23:54	170	96
2000 Jan 8.................	03:06–	S12E02	2004	QS	Sinistral	Yes	. . .	. . .	. . .	No data	. . .	. . .
2000 Jan 15...............	17:48–18:36	S43W58	6502	QS	Sinistral	Limb	. . .	. . .	. . .	19:31	228	75
2000 Apr 11..............	19:48–20:12	S32W44	2304	QS	Sinistral	Limb	. . .	. . .	. . .	20:30	210	45
2000 Apr 21..............	20:24–21:36	S05W03	2684	QS	Sinistral	Yes	. . .	. . .	. . .	. . .	. . .	. . .
2000 Apr 29..............	12:00–12:48	N04E07	2204	QS	Dextral	Yes	C3.0	11:23	S11W06	. . .	. . .	. . .
2000 Jul 7	07:13–13:13[g]	N06W02	2340	QS	Sinistral	Yes	C5.6	08:42	N17E10	10:26	Halo	360
2000 Jul 23	04:24–05:12	S12W06	2408	AR9091	Sinistral	Yes	Optical	. . .	. . .	05:30	Partial halo 161	>181
2000 Jul 30	13:24–14:13	N18W17	2516	QS	Dextral	No	. . .	. . .	. . .	. . .	. . .	
2000 Sep 5................	18:00–20:36	S29E17	3136	QS	Sinistral	Yes	C1.6	21:21	S19W04	. . .	. . .	. . .
2000 Sep 12..............	11:10–11:40	S27W06	5236	AR9160	Sinistral	Yes	M1.0	11:31	S12W18	11:54	Halo	360
2000 Sep 18..............	11:24–12:00	N19W46	6404	QS	Dextral	Yes	. . .	. . .	. . .	12:26	282	35
2000 Sep 27..............	14:48–15:36	S02E45	2706	QS	Sinistral	No	. . .	. . .	. . .	. . .	. . .	. . .
2000 Sep 27..............	19:35–19:50	S31E17	2936	QS	Sinistral	Yes	Optical	. . .	. . .	20:50	192	115
2000 Sep 28..............	06:12–07:13	N12E05	1320	QS	Dextral	Yes	. . .	. . .	. . .	. . .	. . .	. . .
2000 Oct 7	21:13–22:00	N47E27	4384	QS	Dextral	Yes	. . .	. . .	. . .	. . .	. . .	. . .
2000 Oct 15	15:12–17:12	N19W39	3124	QS	Dextral	No	. . .	. . .	. . .	18:26	273	44
2000 Oct 28	19:17–19:54	N18W62	2500	QS	Dextral	Yes	. . .	. . .	. . .	No data	. . .	. . .
2000 Nov 23.............	05:36–06:12	S15W49	3276	QS	Dextral	Yes	C5.4	05:34	S26W40	06:06	Halo	360
2000 Nov 25.............	06:00–07:13	N31W62	3520	QS	Dextral	Limb	. . .	. . .	. . .	07:31	305	44
2001 Jan 24...............	11:12–12:00	N27W07	2448	QS	Dextral	No	. . .	. . .	. . .	. . .	. . .	. . .
2001 Mar 14	10:23–11:09	S28W34	2236	QS	Sinistral	No	. . .	. . .	. . .	12:26	213	26
2001 Apr 2................	10:48–13:13	S22W48	2608	QS	Sinistral	Limb	. . .	. . .	. . .	11:26	270	80
2001 Apr 10..............	11:12–12:36	N19W29	2048	QS	Dextral	Yes	. . .	. . .	. . .	. . .	. . .	. . .
2001 Apr 22..............	23:52–00:30[h]	N37W34	4208	QS	Dextral	Yes	. . .	. . .	. . .	00:42/23	325	69

TABLE 1—*Continued*

	Filaments						Flares			CMEs		
Date (1)	Eruption Time (UT) (2)	Position (3)	Size (arcsec^2) (4)	Type (5)	Chirality (6)	EFR[a] (7)	Class (8)	Time[b] (UT) (9)	Location (10)	Time[c] (UT) (11)	Central P.A.[d] (deg) (12)	AW[e] (deg) (13)
2001 Apr 23	12:03–12:26	S09W28	564	AR9431	Sinistral	Yes	C2.8	12:06	S14W17	12:39	228	91
2001 Apr 23	13:27–14:10	S32W63	2256	QS	...	Limb	...	...	...	...	...	...
2001 Jul 20	03:36–04:12	N35W27	2076	AR9538	Dextral	Yes	B7.6	03:15	...	05:06	357	26
2001 Jul 26	08:48–10:14	N23W81	3044	QS	Sinistral	Limb	...	...	...	...	...	...
2001 Aug 1	20:28–20:56	S29W14	1176	AR9557	Sinistral	No	...	...	...	No data	...	...
2001 Aug 2	19:49–23:48	N40E28	2144	QS	Dextral	Yes	C2.1	18:53	N24E31	00:06/03	...	...
2001 Aug 6	22:36–23:48	N28W94	2836	QS	Dextral	Limb	...	...	...	...	...	...
2001 Sep 15	09:48–10:28	N24W69	4718	QS	Dextral	Limb	...	...	...	...	...	...
2001 Oct 9	10:48–12:24	S26E03	1424	AR9653	Dextral	No	M1.4 1h	10:46	S28E08	11:30	Halo	360
2001 Oct 16	07:13–07:36	N05W74	3644	QS	Sinistral	Limb	...	...	...	...	...	...
2001 Oct 19	16:15–16:25	N18W40	1276	AR9661	Sinistral	Yes	X1.6	16:13	N15W29	16:50	Halo	360
2001 Dec 5	15:48–16:24	N47W54	2060	QS	Dextral	Limb	...	...	...	...	...	...
2002 Jan 6	10:36–11:52	S42W16	2036	QS	...	Limb	...	...	...	...	...	...
2002 Jan 14	22:14–[g]	S21W01	2572	QS	Sinistral	No	...	...	...	No data	...	...
2002 Jan 23	16:27–17:13	N35E18	2092	QS	...	No	...	...	...	...	...	...
2002 Jan 28	10:00–11:00	S32E15	2458	QS	Sinistral	Yes	C4.6	11:05	...	10:54	143	62
2002 Feb 19	23:00–[g]	N53E15	5276	QS	...	Limb	...	...	...	02:54/20	36	41
2002 Mar 5	18:30–19:15	S11W26	5824	QS	Sinistral	No	...	...	...	21:30	215	65
2002 Apr 22	22:37–23:24	S10W03	5380	QS	Sinistral	Yes	...	...	...	00:38/23	213	57
2002 May 21	20:16–20:26	N20E40	737	AR9960	Dextral	Yes	M1.5	21:20	N17E38	21:50	59	117
2002 May 22	03:00–03:36	S12W60	2140	QS	Dextral	Yes	C5.0 2h	04:00	S22W53	03:50	Halo	360
2002 May 24	20:26–20:36	N18E14	218	AR9962	Dextral	No	Optical	20:40	N16E11	...	...	...
2002 Jun 4	17:47–17:57	N14W23	159	AR9974	Dextral	Yes	C1.0	18:06	N22W17	No data	...	...
2002 Jun 10	19:06–20:31	N33W19	3612	QS	Dextral	No	...	...	...	...	...	...
2002 Jun 16	21:13–21:47	S25W45	262	AR9991	...	Yes	C1.2	21:12	...	...	...	...
2002 Jun 17	22:53–23:13	N20E40	475	AR10001	Dextral	No	Optical	22:40	N14E22	...	...	...
2002 Jun 19	20:05–20:20	N20W15	225	AR10000	...	Yes	Optical	...	...	...	...	...
2002 Jul 01	20:32–[g]	S18W09	320	AR10016	Sinistral	Yes	C1.0	21:08	...	...	...	...
2002 Jul 04	16:09–16:19	S18E06	393	AR10019	...	Yes	C3.4	16:21	S19E06	18:54	180	45
2002 Jul 07	17:00–17:26	N08W49	4560	QS	Dextral	Yes	Optical	...	...	18:06	293	65
2002 Jul 13	10:28–11:12	S24E28	2488	QS	Sinistral	Yes	...	...	...	11:30	147	40
2002 Jul 21	16:11–16:31	S16E02	472	QS	Sinistral	Yes	Optical	15:47	S09W16	...	...	...
2002 Jul 23	14:30–18:20	N53W54	8148	QS	Dextral	Limb	...	...	...	18:06	342	56
2002 Jul 26	15:37–15:48	N10W24	1184	AR10046	Sinistral	Yes	Optical	...	...	...	...	...
2002 Jul 29	07:13–10:29	N32W40	4108	QS	Dextral	Yes	...	...	...	11:06	360	150
2002 Aug 6	16:59–17:19	S31W35	9900	QS	Sinistral	No	...	...	...	18:25	218	134
2002 Aug 14	19:34–20:28	N10E17	408	AR10067	Dextral	Yes	M1.4	18:04	N10E23	...	...	...
2002 Aug 18	18:18–18:37	S09W17	596	QS	...	Yes	C8.7	20:18	S07W20	21:54	203	140
2002 Aug 20	23:42–00:04[h]	N55W10	3692	QS	Dextral	Limb	...	...	...	...	...	...
2002 Sep 15	19:52–20:17	N33E45	2140	QS	Dextral	Yes	...	...	...	21:30	59	41
2002 Sep 18	23:04–23:29	S22E03	2152	AR10119	Sinistral	No	C1.0	21:48	...	...	...	...
2002 Sep 21	20:11–20:36	S11W22	408	AR10123	Sinistral	Yes	C2.6	20:34	S16W19	...	...	...
2002 Sep 22	10:28–11:48	N26W54	6700	QS	Dextral	Limb	...	...	...	11:30	287	43
2002 Sep 29	22:20–01:25[h]	S26W00	2416	QS	Sinistral	No	...	...	...	...	...	...
2002 Sep 29	22:20–01:25[h]	S13E21	2400	QS	Sinistral	Yes	...	...	...	23:54	146	22

TABLE 1—*Continued*

	Filaments						Flares			CMEs		
Date (1)	Eruption Time (UT) (2)	Position (3)	Size (arcsec^2) (4)	Type (5)	Chirality (6)	EFR[a] (7)	Class (8)	Time[b] (UT) (9)	Location (10)	Time[c] (UT) (11)	Central P.A.[d] (deg) (12)	AW[e] (deg) (13)
2002 Sep 30	06:36–08:24	S12W87	1824	QS	Sinistral	Limb	...	...	...	...	...	...
2002 Oct 10	19:03–20:08	N29W01	812	QS	Dextral	No	...	...	...	No data	...	...
2002 Oct 29	23:28–01:13[h]	S14W40	3584	QS	...	Yes	...	...	...	...	...	...
2002 Nov 19	21:00–00:00	S03W57	2800	QS	Sinistral	Limb	...	...	...	...	...	...
2002 Nov 19	23:00–00:00	S47W63	2196	QS	Sinistral	Limb	...	...	...	...	...	...
2002 Dec 29	01:13–02:36	S31W12	2584	QS	Sinistral	Yes	...	...	...	...	...	...
2003 Jan 20	15:12–18:24	N40W30	5000	QS	Dextral	Limb	Optical	...	...	18:30	315	105
2003 Jan 20	12:48–13:13	S02W36	3656	QS	Sinistral	No	...	...	...	...	...	...
2003 Jan 20	20:24–21:12	N25E55	6250	QS	Dextral	Yes	Optical	...	...	21:30	58	166
2003 Jan 30	08:12–09:33	N18W00	2480	QS	Dextral	No	Optical	...	...	10:06	Partial halo 238	149
2003 Mar 25	17:15–[g]	N37W13	4076	QS	...	Limb	...	...	...	19:31	0	65
2003 Apr 26	20:33–21:18	N00E48	4160	QS	Dextral	Limb	...	...	...	21:50	48	166
2003 Jun 11	17:56–18:56	S42E08	5088	QS	Sinistral	No	M1.8	17:27	S16E23	No data	...	...
2003 Jun 14	03:24–04:12	N24W36	4328	QS	Dextral	Yes	Optical	...	...	...	...	...
2003 Aug 5	17:54–18:34	N15W21	6084	QS	Dextral	Yes	...	...	...	19:31	336	57
2003 Sep 24	06:00–07:13	S20W27	5952	QS	Sinistral	No	...	...	...	...	...	...
2003 Oct 26	00:36–01:13	S22W66	2188	QS	Sinistral	Limb	C3.2	00:45	...	01:31	256	75

Note.—Table 1 is also available in machine-readable form in the electronic edition of the *Astrophysical Journal*.
[a] EFR: emerging flux region.
[b] Flare onset time (UT).
[c] First C2 appearance Ttime (UT).
[d] Central P.A.: central position angle measured from solar north in degrees (counter-clockwise), provided by LASCO CME catalog.
[e] AW: angular width, provided by LASCO CME catalog.
[f] Limb: near limb.
[g] Data gap.
[h] Next day.

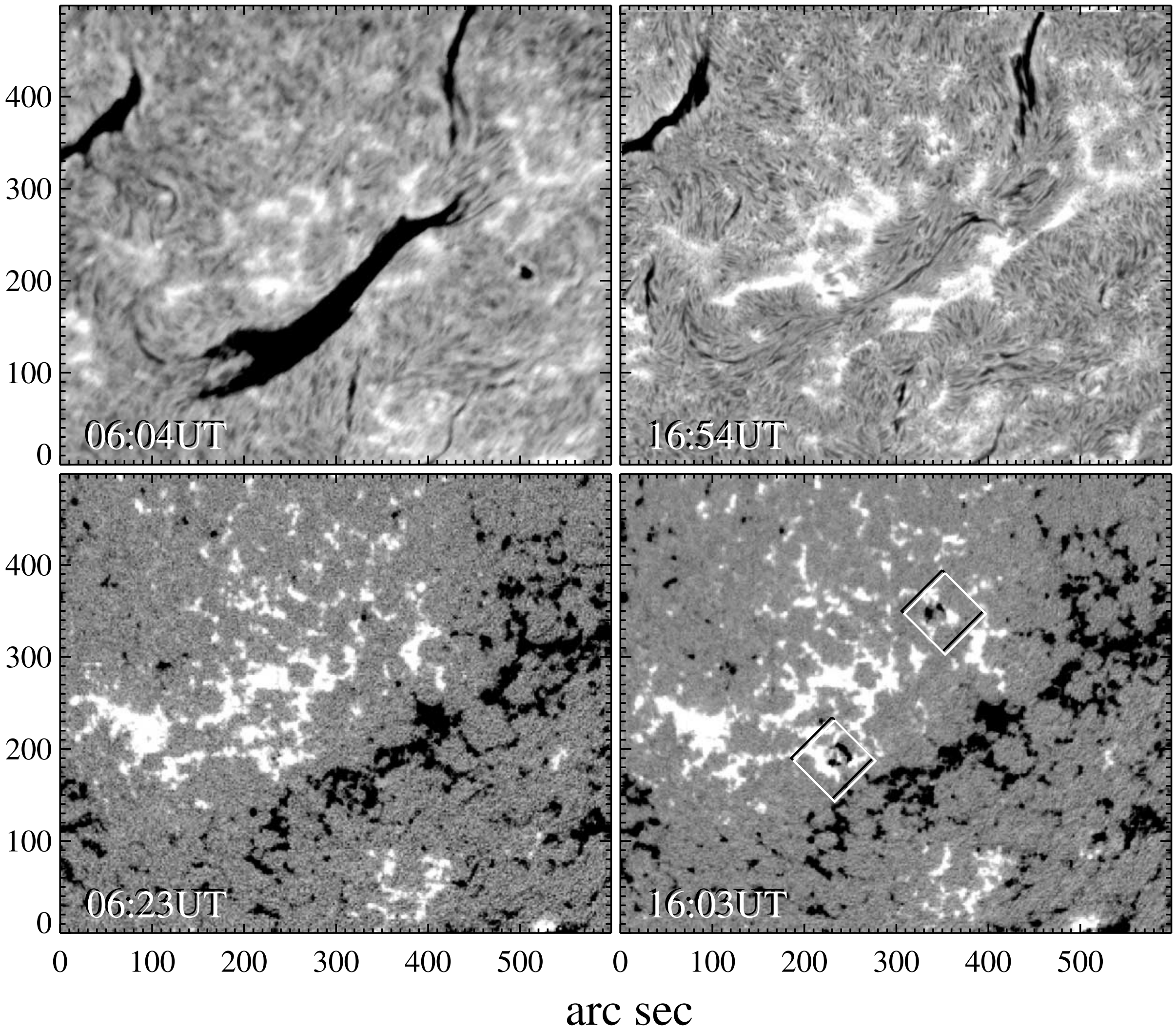

FIG. 1.—Two bipoles emerged on 2000 September 12 alongside an eruptive filament. The top two panels are Hα images taken before and after the eruption obtained at KSO and BBSO, respectively. The bottom two panels are MDI magnetograms. The two bipoles, as indicated by the square boxes, emerged on the positive polarity side of the filament.

1. *Type.*—Active region filaments form in polarity reversal regions of active region complexes, whereas quiescent filaments are usually found in quiet-Sun areas along polarity inversion lines between large-scale areas of opposite polarity (Feynman & Martin 1995).

2. *Chirality.*—Chirality describes the handedness of filaments, and it contains important information of the surrounding magnetic field. When viewed from the positive polarity side, the axial field of a dextral (sinistral) filament points to the right (left). Dextral and sinistral filaments can be recognized even without knowing the polarity on either side of the filaments. Martin et al. (1993) discovered a no-exception correlation between chirality of filament channels, filaments, and their overlying coronal arcades: all dextral filaments are right-bearing and lying under left-skewed arcades, while all sinistral filaments are left-bearing and lying under right-skewed arcades (for a review, see Martin 1998). We determined the chirality by examining high-resolution BBSO Hα images. If the filament barbs bear off to the right (left) of the filament's main axis then the filament is dextral (sinistral). In some cases the chirality of a filament could not be determined as a result of an obscure or complex Hα structure, which is indicated by the ellipses in column (6) of Table 1.

3. *Emerging flux regions.*—Since the sensitivity of longitudinal magnetograms decreases near the limb, we used "Limb" when the normalized distance from solar disk center is larger than 0.6 $R_\odot$ and new flux emergence could not clearly be established.

4. *Flares.*—As mentioned in § 3, we used Hα and EIT full-disk observations, *GOES* soft X-ray flux profiles, and SGD solar event reports to identify flares associated with filament eruptions. The term "optical" refers to a flare visible in Hα full-disk images, which is either inconspicuous in soft X-rays flux profiles or is of an insufficient magnitude to be officially classified as a flare.

5. *CMEs.*—The first appearance in the LASCO C2 FOV, the central position angle (P.A.), and angular width are provided in the LASCO CME catalog. In column (11) of Table 1, we used ellipses to indicate that we could not find a CME associated with the filament eruption; "no data" refers to the few occasions when no LASCO data were available.

5. DISCUSSION

5.1. *Chirality*

Our statistics of filament chirality shows that filaments in the northern hemisphere are predominantly dextral, while filaments in the southern hemisphere are sinistral. This agrees with the observations of Martin et al. (1993), who report that both solar hemispheres have a distinct chirality. This hemispheric pattern seems to suggest that differential rotation and/or Coriolis force participate in twisting the magnetic structures (Priest et al. 1996).

A one-to-one correspondence between filament chirality and the sign of magnetic helicity in interplanetary CMEs (ICMEs) has been reported in a number of studies: dextral (sinistral) filaments contain left-handed (right-handed), negative (positive) magnetic helicity (Bothmer & Schwenn 1994; Rust & Martin 1994; McAllister & Martin 2000; Yurchyshyn et al. 2001). Also, Leamon et al. (2002) reported a 95% correspondence between the helicity of the magnetic clouds associated with eruption of filaments and the heliosphere in which those filaments were located. The sign of magnetic helicity in an active region can be used to predict the orientation of the magnetic field associated with a CME and, furthermore, the likelihood of a geomagnetic storm (Yurchyshyn et al. 2001).

5.2. *New Flux Emergence*

EFRs often occur in active regions and play a significant role in filament eruptions and flare production (Liggett & Zirin 1985; Feynman & Martin 1995). The relation between filament eruptions and new flux emergence is shown in column (7) of Table 1. Figure 1 shows an example of two magnetic bipoles (enclosed in the boxes) emerging alongside a filament on 2000 September 12. The two top panels are Hα images obtained at KSO and BBSO, respectively, taken before and after the filament eruption. The eruption began at about 11:10 UT and was followed by a classical two-ribbon flare. Examining a sequence of MDI magnetograms, we found that these bipoles started to appear at 06:23 UT on the positive polarity side of the filament and continued to develop after the eruption.

After excluding events located far away from the disk center, where the detection of new flux emergence was difficult, we have obtained a sample of 80 eruptive filaments suitable to study the magnetic field evolution. The 54 (68%) events were accompanied by new flux emergence. The new flux usually appeared in the vicinity of an eruptive filament and within 15 hr prior to the filament eruption. Our study also showed that new flux emergence occurred in both active and quiet-Sun regions. Therefore, we conclude in agreement with Wang & Sheeley (1999) that new flux emergence plays an important role in destabilizing filaments.

5.3. *Flares and CMEs*

Eight events without the corresponding LASCO data were listed in Table 1 but excluded from Figure 2. The top panel of Figure 2 shows the heliographic latitude of flares and CMEs that were associated with eruptive filaments. We used asterisks to indicate filament eruptions associated with neither flares nor CMEs. Diamonds denote the occurrence of a flare and triangles show the occurrence of CMEs. Squares were used in cases in which both flares and CMEs were detected. Of 98 events, 55 (56%) of the filament eruptions were accompanied by CMEs.

The above number is considerably weaker than the 94% association reported for EPs reported by Gilbert et al. (2000) and the 83% for radial events by Gopalswamy et al. (2003), but much higher than the 10%–30% range given by Yang & Wang (2002). This apparent difference can be explained as follows: Gilbert et al. (2000) and Gopalswamy et al. (2003) considered only prominence eruptions, i.e., limb events. In contrast to

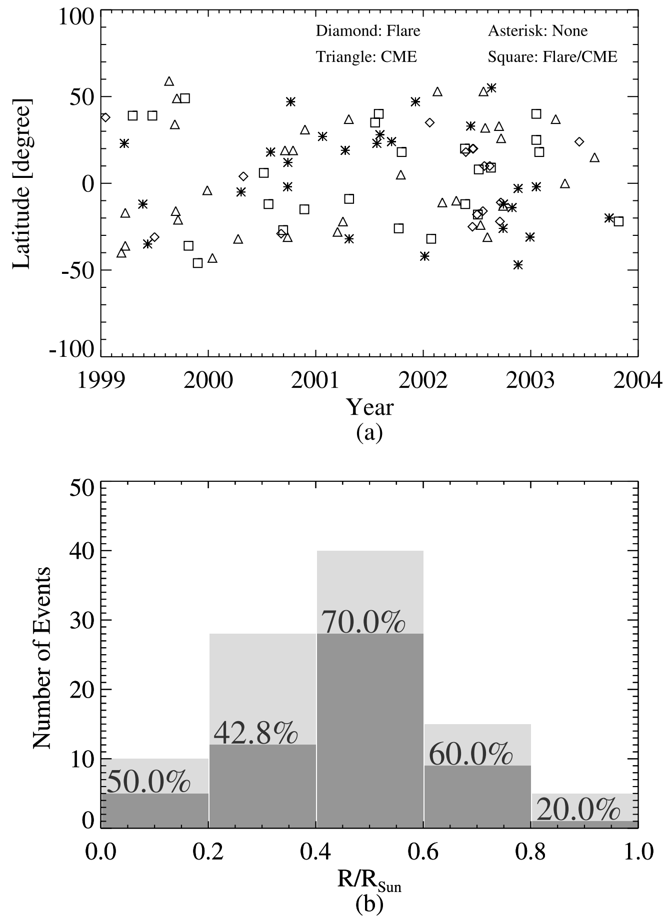

Fig. 2.—*Top*: Latitudinal distribution of eruptive filaments and their overall relation to flares and CMEs. Asterisks denote filament eruptions, which were associated with neither flares nor CMEs. Diamonds refer to flares, triangles to CMEs, and squares to both flares and CMEs, which were related to filament eruptions. *Bottom*: Frequency distribution of filament eruptions and associated CMEs as function of their distance from disk center. The histogram in light gray corresponds to filament eruptions, and the histogram in dark gray represents the associated CMEs, where the fraction of CMEs to filament eruptions is given for each interval.

these studies, the events listed in Table 1 are mainly disk events. It is likely for some disk events that the associated CMEs are very faint and could not be detected by LASCO. The low CME association reported by Yang & Wang (2002) was most probably due to the fact that they did not distinguish between filament disappearances and eruptions, while we explicitly excluded disappearances. Moreover, the size criteria that they employed were different from ours. They included all disappearance events, while we mainly considered filaments with a size of at least 2000 arcsec^2. Thus, the Yang & Wang (2002) results provide a lower estimate, since smaller eruptive events might be associated with fainter CMEs and therefore are more likely to be missed in LASCO data.

The bottom panel of Figure 2 shows the distribution of eruptive filaments as a function of distance from the solar disk center. The light gray bars represent the number of filament events, while the dark bars are the number of associated CMEs. The fraction of CMEs to filament eruptions is given in percent for each bar in the histogram. The highest fraction of 70% occurs in the range of $R = 0.4-0.6\ R_\odot$.

In Table 2 we distinguish between active region and quiescent filament eruptions and relate them to flares and CMEs. Here the term "flare" refers to both optical Hα and *GOES*

TABLE 2
ACTIVE REGION AND QUIESCENT FILAMENTS AND THEIR RELATION TO FLARES AND CMEs

Filament Type	Total	With Flare	Without Flare	With CME	Without CME	No LASCO Data
Active region filaments	21	20 (95%)	1 (5%)	9 (43%)	10 (48%)	2 (9%)
Quiescent filaments	85	23 (27%)	62 (73%)	46 (54%)	33 (39%)	6 (7%)
Total	106	43 (41%)	63 (59%)	55 (52%)	43 (40%)	8 (8%)

X-ray flares. Active region filament eruptions are more likely to be associated with flares (95%) than quiescent filament eruptions (28%), since large-scale magnetic shear and strong magnetic field in an active region can store plenty of magnetic energy to be released in flares (Hagyard et al. 1984). Of a total of 85 quiescent filament eruptions, 46 (54%) are accompanied by CMEs, while only 23 (27%) events produce flares. This eminent relation between filament eruptions and CMEs suggests that filament eruptions in a quiescent region or at the periphery of an active region will more likely be associated with a CME that is not itself associated with a flare. The above flare association could, quite possibly, be higher if we consider the fact that some flares during the eruption may be too weak to be observed in either *GOES* soft X-rays or Hα.

5.4. *Halo CMEs*

Halo CMEs have received considerable attention, since they are responsible for major interplanetary disturbances and geomagnetic storms (Burlaga et al. 1981; Wilson & Hildner 1984). Because the southwardly component B_z of the interplanetary magnetic field (IMF) is responsible for magnetic reconnection between the IMF and Earth's magnetic field, it plays an important role in determining the amount of particle energy that is injected into the magnetosphere (Arnold 1971; Akasofu 1981). Usually, the presence of a strong and prolonged southward-directed IMF is associated with enhanced geomagnetic activity. For ICMEs with their axial magnetic field oriented along the north-south line, the magnitude of the southward component is largely determined by this axial field and the sign of magnetic helicity plays a minor role. At the same time, for CMEs with east-west oriented axial fields, both the sign and magnitude of its southward component are largely determined by the magnetic helicity of the CME (Yurchyshyn et al. 2001).

Table 3 summarizes results for seven eruptive filaments, taken from Table 1, associated with halo CMEs and geomagnetic storms. The content in the first four columns is in accordance with that in Table 1, while column (5) shows the orientation of CMEs, which is assumed to be the same as the orientation of the axial magnetic field of the corresponding filaments. The linear fit speed of the CMEs, which was taken from the *SOHO*/LASCO CME Catalog, is listed in column (6). In the last three columns, we present the transit time of the ICME and the peak values of the Dst and Kp indices during the subsequent geomagnetic storms. Four of seven halo CMEs were associated with geomagnetic storms with the peak Dst values ranging between −70 and −187 nT. The peak Kp values were found to be between 5 and 8 nT. All but one geomagnetic event could be predicted on the basis of the chirality of the CME's magnetic field. The exception is the CME on 2001 October 19. Considering its west-east directed axial magnetic field and sinistral chirality of the associated filament, the leading edge of the magnetic cloud should have had a northward-directed component, and thus this event should not be associated with a significant geomagnetic activity. However, a strong storm occurred 2 days after the CME launched. Examination of Advanced Composition Explorer (ACE) magnetometer data revealed that the magnetic field at the leading edge was indeed northward-directed, and the storm was caused by a strong southward component in the shock region preceding the interplanetary ejecta.

6. SUMMARY

In summary, we studied phenomena of solar activity associated with filament eruptions, which were automatically detected by BBSO's "filament disappearance report." A total of 106 major filament eruption events, identified from 1999

TABLE 3
FILAMENT ERUPTIONS ASSOCIATED WITH HALO CMEs, AND THEIR GEOEFFECTIVENESS

	FILAMENTS			HALO CMEs		GEOMAGNETIC STORMS		
DATE (1)	Type (2)	Position (3)	Chirality (4)	Orientation (5)	Speed[a] (km s^{-1}) (6)	Transit Time[b] (days) (7)	Peak Dst[c] (nT) (8)	Peak Kp[d] (nT) (9)
1999 Sep 20	QS	S21E01	Sinistral	Southeast-northwest	604	2.8	−173	8
2000 Jul 7	QS	N06W02	Sinistral	South-north	453	. . .	. . .	. . .
2000 Sep 12	AR	S27W06	Sinistral	Southeast-northwest	1550	. . .	. . .	. . .
2000 Nov 23	QS	S15W49	Dextral	East-west	492	. . .	. . .	. . .
2001 Oct 9	AR	S26E03	Dextral	West-east	973	2.4	−70	5
2001 Oct 19	AR	N18W40	Sinistral	West-east	901	2.3	−187	7
2002 May 22	QS	S12W60	Dextral	Northwest-southeast	1494	1.6	−109	8

[a] Linear fit speed from *SOHO*/LASCO CME Catalog.
[b] Transit time from solar onset to storm peak.
[c] Dst = −50: moderate storm; Dst = −100: intense storm.
[d] Kp = 5: moderate storm; Kp = 6: intense storm.

January 1 to 2003 December 31, were included in the sample for this study.

1. Excluding eight events without corresponding LASCO data, 55 (56%) of 98 events were associated with CMEs. This CME association is lower than the 94% fraction reported by Gilbert et al. (2000) and the 84% fraction by Gopalswamy et al. (2003), but it is considerably higher than the 10%–30% value association found by Yang & Wang (2002).

2. Active region filament eruptions have a considerably higher flare association (95%) than quiescent filament eruptions with only 27% association. On the other hand, quiescent filament eruptions (85 events) are more likely to be accompanied by CMEs than flares.

3. Of 80 disk events, 54 (68%) events were associated with new flux emergence. This suggests that new flux emergence plays an important role in destabilizing filaments.

4. We determined the chirality and the orientation of magnetic fields associated with seven halo CMEs and their relationship to geomagnetic storms. Our results seem to support earlier reports that the geoeffectiveness of a halo CME can be predicted from its orientation and the sign of magnetic helicity (Yurchyshyn et al. 2001).

We thank the referee for providing constructive comments, and we thank Carsten Denker for his help in improving the contents of this paper. We thank the ACE MAG instrument team and the ACE Science Center for providing the ACE data. We acknowledge the use of geomagnetic data from the World Data Center for Geomagnetism in Kyoto. The CME catalog is generated and maintained by NASA and The Catholic University of America in cooperation with the Naval Research Laboratory. *SOHO* is a project of international collaboration between ESA and NASA. This research is supported by NSF grants ATM-0313591 and ATM-0233931, and NASA grants NAG5-12733 and NAG5-13661.

REFERENCES

Akasofu, S. I. 1981, Space Sci. Rev., 28, 121
Arnold, R. J. 1971, J. Geophys. Res., 76, 5189
Bothmer, V., & Schwenn, R. 1994, Space Sci. Rev., 70, 215
Brueckner, G. E., et al. 1995, Sol. Phys., 162, 357
Burlaga, L. F., Sittler, E., Mariani, F., & Schwenn, R. 1981, J. Geophys. Res., 86, 6673
Cane, H. V., Richardson, I. G., & St. Cyr, O. C. 2000, Geophys. Res. Lett., 27, 3591
Delaboudinière, J.-P., et al. 1995, Sol. Phys., 162, 291
Denker, C., Johannesson, A., Goode, P. R., Marquette, W., Wang, H., & Zirin, H. 1999, Sol. Phys., 184, 87
Feynman, J., & Martin, S. F. 1995, J. Geophys. Res., 100, 3355
Gao, J., Wang, H., & Zhou, M. 2002, Sol. Phys., 205, 93
Gilbert, H. R., Holzer, T. E., Burkepile, J. T., & Hundhausen, A. J. 2000, ApJ, 537, 503
Gopalswamy, N., Shimojo, M., Lu, W., Yashiro, S., Shibasaki, K., & Howard, R. A. 2003, ApJ, 586, 562
Gosling, J. T., McComas, D. J., Phillips, J. L., & Bame, S. J. 1991, J. Geophys. Res., 96, 7831
Hagyard, M. J., Moore, R. L., & Emslie, A. G. 1984, Adv. Space Res., 4, 71
Leamon, R. J., Canfield, R. C., & Pevtsov, A. A. 2002, J. Geophys. Res., 107, 1
Liggett, M., & Zirin, H. 1985, Sol. Phys., 97, 51
Martin, S. F. 1998, Sol. Phys., 182, 107
Martin, S. F., Bilimoria, R., & Tracadas, P. W. 1993, AAS Meeting, 24, 19.07
McAllister, H., & Martin, S. F. 2000, Adv. Space Res., 26, 469
Mouradian, Z., Sour-Escaut, I., & Pojoga, S. 1995, Sol. Phys., 158, 269
Priest, E. R., Van Ballegooijen, A. A., & MacKay, D. H. 1996, ApJ, 460, 530
Rust, D. H., & Martin, S. F. 1994, in ASP Conf. Ser. 68, Solar Active Region Evolution: Comparing Models with Observations, ed. K. S. Balasubramaniam & G. W. Simon (San Francisco: ASP), 337
Scherrer, P. H., et al. 1995, Sol. Phys., 162, 129
Steinegger, M., et al. 2000, in The Solar Cycle and Terrestrial Climate, ed. A. Wilson (ESA SP-463; Noordwijk: ESA), 617
Wang, Y. M., & Sheeley, N. R., Jr. 1999, ApJ, 510, L157
Webb, D. F., Cliver, E. W., Crooker, N. U., St. Cyr, O. C., & Thompson, B. J. 2000, J. Geophys. Res., 105, 7491
Webb, D. F., & Hundhausen, A. J. 1987, Sol. Phys., 108, 383
Wilson, R. M., & Hildner, E. 1984, Sol. Phys., 91, 169
Yang, G., & Wang, H. 2002, in COSPAR Colloq. Ser. 14, Solar-Terrestrial Magnetic Activity and Space Environment, ed. H. Wang & R. Xu (Boston: Pergamon), 113
Yurchyshyn, V. B., Wang, H., Goode, P. R., & Deng, Y. 2001, ApJ, 563, 381